SISSA

Restrictions on the lifetime of sterile neutrinos from primordial nucleosynthesis

To cite this article: Oleg Ruchayskiy and Artem Ivashko JCAP10(2012)014

View the article online for updates and enhancements.

Restrictions on the lifetime of sterile neutrinos from primordial nucleosynthesis

Oleg Ruchayskiy[a] **and Artem Ivashko**[b,c]

[a]Physics Department, Theory Division, CERN,
 CH-1211 Geneva 23, Switzerland

[b]Instituut-Lorentz for Theoretical Physics, Universiteit Leiden,
 Niels Bohrweg 2, Leiden, The Netherlands

[c]Department of Physics, Kiev National Taras Shevchenko University,
 Glushkov str. 2 building 6, Kiev, 03022, Ukraine

E-mail: oleg.ruchayskiy@epfl.ch, ivashko@lorentz.leidenuniv.nl

Abstract. We analyze the influence of sterile neutrinos with the masses in the MeV range on the primordial abundances of Helium-4 and Deuterium. We solve explicitly the Boltzmann equations for all particle species, taking into account neutrino flavour oscillations and demonstrate that the abundances are sensitive *mostly* to the sterile neutrino lifetime and only weakly to the way the active-sterile mixing is distributed between flavours. The decay of these particles also perturbs the spectra of (decoupled) neutrinos and heats photons, changing the ratio of neutrino to photon energy density, that can be interpreted as extra neutrino species at the recombination epoch. We derive upper bounds on the lifetime of sterile neutrinos based on both astrophysical and cosmological measurements of Helium-4 and Deuterium. We also demonstrate that the recent results of Izotov & Thuan [1], who find 2σ higher than predicted by the standard primordial nucleosynthesis value of Helium-4 abundance, are consistent with the presence in the plasma of sterile neutrinos with the lifetime 0.01–2 seconds.

JCAP10(2012)014

Contents

1   Introduction

The characteristic feature of the physical processes in the early Universe is a peculiar interplay of gravity and microscopic physics. Gravity introduces the *Hubble time parameter* τ_H that indicates the timescale on which the global properties of the Universe (geometry, temperature, etc.) change significantly. The Hubble time is determined solely by the energy density of the matter filling the space. The microscopic matter constituents, particles, are involved in the interaction processes, that are believed to be described fundamentally by three known forces — electromagnetic, weak and strong. As long as the timescale τ of any given microscopic physical process is much smaller than τ_H, the expansion can be neglected on that timescale. If time τ is enough to establish thermal equilibrium between the particles, then the equilibrium it maintained in the course of the Universe expansion, while $\tau \ll \tau_H$ holds. When this inequality ceases to hold, the state of equilibrium is lost. The main reason for that is that interparticle distances become larger, while the corresponding densities become lower, hence interactions are less likely to occur.

In this paper we are consider the formation of light nuclei in the primordial environment — Big Bang nucleosynthesis (BBN). All three fundamental interactions are important for this phenomenon, all playing different roles. Charged particles together with photons are subject to electromagnetic forces and the equilibration timescale of corresponding processes is tiny

with respect to the expansion time. Therefore the particles are kept in thermal equilibrium at the common temperature T. Due to expansion the temperature is *decreasing* with time. The equilibration time of the weak interactions changes abruptly so that at $T \gtrsim$ few MeV weakly interacting neutral particles (neutrinos and neutrons) stay in equilibrium, while at lower temperatures they fall out of it (freeze out).

At high temperatures processes like $n + \nu_e \rightarrow p + e^-$ maintain *chemical* equilibrium, that is the neutron-to-proton conversion exhibits the same finite intensity as the opposite processes. Chemical and thermal equilibria are interconnected, so they are lost simultaneously, when neutron-to-proton ratio freezes out. Finally, the strong interactions are responsible for the production of nuclei comprising more than one nucleon. The most important fusion reaction for the formation of the first nucleus, deuteron, $n + p \rightarrow D$, *releases* energy of at least the binding energy of deuteron $E_D \approx 2.2$ MeV, and proceeds effectively in dense primordial medium. At temperatures of the order of E_D, however, energetic photons collide with deuteron and lead to its destruction. As baryon density is much lower than the density of photons [2], there are *many* photons with energies much higher than E_D that collide with deuterons and hence postpone the production of the significant deuteron density until the temperature when the photodissociation is not effective anymore, $T \simeq 80$ keV, much lower than the binding energy. The net abundance of deuterium is, however, non-zero at all times till this moment and is given by the equilibrium Boltzmann distribution. Deuterium that is created at lower temperatures, serves as a fuel for the formation of ^{3}He, ^{4}He and other nuclides.

Although the times of elements' production and the moment of the departure from the chemical $p - n$ equilibrium are well-separated, the former process is very sensitive to the latter. Firstly, the details of the freeze-out set the ratio of the neutron to proton densities, and secondly, the time elapsed between the two moments determines the fraction of neutrons that have decayed since then (recalling that neutron is an unstable particle).

The seminal ideas of the primordial synthesis of light elements were first outlined in the so-called $\alpha\beta\gamma$ paper, [3], published in the late 1940s. Since then the theory of Big Bang nucleosynthesis has evolved and its main predictions were confirmed, making it a well-developed model from both theoretical and observational points of view. A lot of reviews of the standard BBN scenario and its implication for particle physics models exist (see e.g. [4–6]).

The predictions of the primordial nucleosynthesis can change once one replaces the Standard Model of particle physics underlying the processes considered so far by some of its "beyond the Standard Model" (BSM) extensions. Therefore the BBN plays the role of a benchmark for testing physical models.

In this paper we investigate the influence of *sterile neutrinos* on primordial nucleosynthesis. Sterile neutrinos are hypothetical massive *super-weakly-interacting* particles (see e.g. [7, 8] for reviews), as opposed to their weakly-interacting counterparts — ordinary Standard Model neutrinos ν_e, ν_μ, ν_τ, that are called "active" in this context. Sterile neutrinos carry no charges with respect to the Standard Model gauge groups (hence the name), but via their quadratic *mixing* to active neutrinos they effectively participate in weak reactions and at energies much below the mass of the W-boson their interaction can be described by the analog of the Fermi theory with the Fermi coupling constant G_F replaced by $G_F \times \vartheta_\alpha$, where the *active-sterile mixing angle* $\vartheta_\alpha \ll 1$ (see figure 1). Here α is a flavour index, $\alpha = e, \mu, \tau$, indicating that sterile neutrino can mix differently with neutrinos of different flavours. Massive sterile neutrinos can decay, but due to their feeble interaction strength their lifetime can be of order seconds (even for masses as large as MeV). The decay products of the sterile neutrinos are injected into the primordial environment, increasing its temperature and shifting the chemical equilibrium.
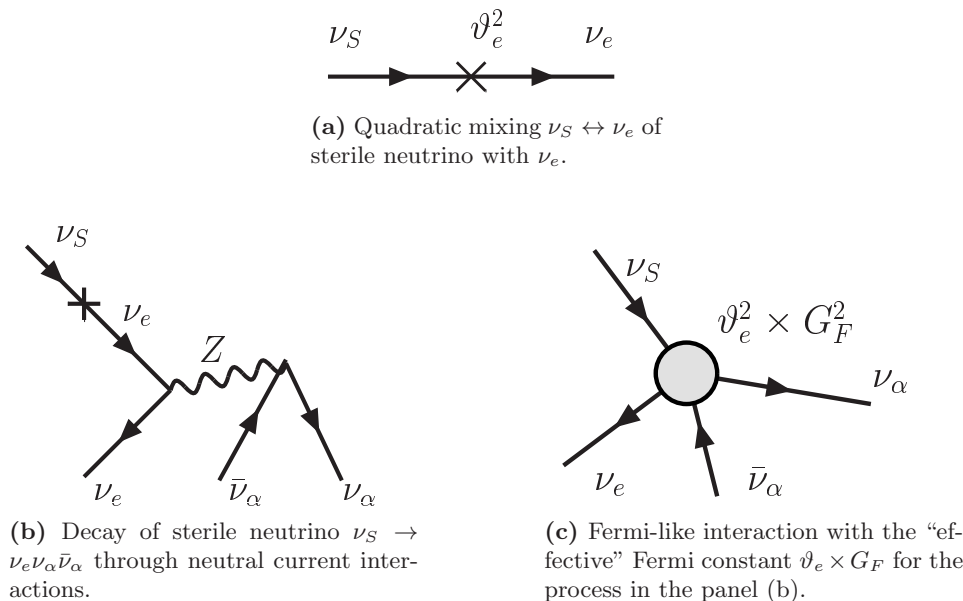
(a) Quadratic mixing $\nu_S \leftrightarrow \nu_e$ of sterile neutrino with ν_e.

(b) Decay of sterile neutrino $\nu_S \rightarrow \nu_e \nu_\alpha \bar{\nu}_\alpha$ through neutral current interactions.

(c) Fermi-like interaction with the "effective" Fermi constant $\vartheta_e \times G_F$ for the process in the panel (b).

Figure 1. Fermi-like super-weak interactions of sterile neutrino.

In this work we concentrate on sterile neutrinos with the masses in the MeV range, motivated by the recent observations [9–13] that particles with such masses can be responsible simultaneously for neutrino oscillations and generation of baryon and lepton asymmetry of the Universe and can influence the subsequent generation of dark matter [14]. The corresponding model has been dubbed νMSM (*Neutrino Minimal Standard Model*, see [7] for review).

Several works had previously considered the influence of MeV-scale particles on primordial nucleosynthesis. Compared to the refs. [15, 16] this paper accounts for the neutrino flavour oscillations in the plasma and employs more accurate strategy of solving Boltzmann equations, which results in the revision of the bounds of [15, 16] (see section 4 for detailed comparison). The authors of [17] developed a new code that can perform treatment of active and sterile neutrinos with arbitrary distribution functions, non-zero lepton asymmetry, etc. However, as of time of writing this code has not been made publicly available and the ref. [17] did not derive bounds on sterile neutrino parameters. The work [18] concentrated on the bounds that cosmic microwave background measurements could provide on decaying sterile neutrinos with the masses 100–500 MeV, leaving BBN analysis for the future work. A number of other works ([19–23]) analyzed the influence of decaying MeV particles on BBN. We compare with them in the corresponding parts of the paper.

The paper is organized as follows. We explain the modifications of the standard BBN computations due to the presence of sterile neutrinos in the plasma and describe our numerical procedure in section 2. The results are summarized in section 3. We conclude in section 4. Appendixes A–C provide the details of our numerical procedure.

2 Big Bang nucleosynthesis with sterile neutrinos

The section below summarizes our setup for the BBN analysis with decaying particles. The notations and conventions closely follow the series of works [16, 24, 25].

We will be interested only in the tree-level Fermi interactions of sterile neutrinos with the primordial plasma. In this case the interaction is fully determined by the squares of their mixing angles. We will consider one Majorana particle with 4 degrees of freedom[1] and three *active-sterile mixing angles* ϑ_α^2. Matrix elements of interactions of sterile neutrinos with the Standard Model particles are summarized in appendix B (tables 3–4).

We consider in this work only sterile neutrinos with the masses in the range $1\,\text{MeV} < M_s < M_\pi \approx 140\,\text{MeV}$. For heavier particles, two-particle decay channels appear (e.g. $\nu_S \to \pi_0\nu_\alpha, \pi^\pm e^\mp$) and our procedure of solving Boltzmann equations (described below) should be significantly modified. The lower bound was chosen to be around 1 MeV by the following considerations. The sterile neutrino lifetime τ_s is [26]

$$\tau_s^{-1} = \Gamma_s = \frac{G_F^2 M_s^5}{96\pi^3} \left[(1 + \tilde{g}_L^2 + g_R^2)(\vartheta_\mu^2 + \vartheta_\tau^2) + (1 + g_L^2 + g_R^2)\vartheta_e^2\right]$$
$$\approx 6.9\,\text{sec}^{-1} \left(\frac{M_s}{10\,\text{MeV}}\right)^5 \left[1.6\,\vartheta_e^2 + 1.13(\vartheta_\mu^2 + \vartheta_\tau^2)\right] \tag{2.1}$$

where θ_W is the Weinberg's angle and $g_R = \sin^2\theta_W \approx 0.23$, $g_L = \frac{1}{2} + \sin^2\theta_W$, $\tilde{g}_L = -\frac{1}{2} + \sin^2\theta_W$.[2] From this expression one sees that sterile neutrinos lighter than about 2 MeV have lifetime of at least several hundred seconds even for very large mixing angles $\vartheta \sim 1$. Therefore, such particles survive till the onset of the BBN, and freeze-out at temperatures $T \sim 2 - 3\,\text{MeV}$. They would be relativistic at that time, i.e. their average momentum would be of the order of temperature, $\langle p \rangle \sim T$, and their contribution to the number of relativistic neutrino species would be significant, $\Delta N_{\text{eff}} \simeq 2$. In the course of the Universe expansion $\langle p \rangle$ would scale as temperature due to the gravitational redshift, and at some point would become smaller than the mass of sterile neutrino. At that moment the energy density of sterile neutrinos would start to change with expansion as a^{-3} rather than a^{-4} (where a is a scale-factor) so that the contribution of these massive particles to the energy density would quickly become dominant, making $N_{\text{eff}} \gg 1$ (or could even overclose the Universe) before the production of light elements starts. It contradicts the current bound that puts $N_{\text{eff}} = 3.74^{+0.8}_{-0.7} \pm 0.06(\text{syst})$ at 2σ [1].[3]

Additionally, in the νMSM the successful baryogenesis is possible only for the masses of sterile neutrinos above few MeV [11, 13]. Therefore we restrict the analysis to the region of masses higher than 1 MeV.

2.1 Expanding Universe and distributions of particles

We consider expansion of the homogeneous and isotropic Universe with the flat Friedmann-Robertson-Walker metric in the form $ds^2 = dt^2 - a^2 d\vec{x}^2$, where $a = a(t)$ is a time-dependent scale factor, whose evolution is described by the Friedmann equation

$$H \equiv \frac{\dot{a}}{a} = \sqrt{\frac{8\pi G_N}{3}\rho} \ , \tag{2.2}$$

---

[1]This number corresponds to $g_s = 2$ of additional chiral singlets (i.e. "neutrino-like" species). Actual number of degrees of freedom is of course twice larger: dof $= 2 \times g_s = 4$, because every chiral fermion has 2 different helicity states.

[2]The expression (2.1) is for Majorana particle. For Dirac particle the lifetime would be twice larger.

[3]Here the systematic error is due to the different values of neutron lifetime between the average value from Particle Data group, [27] and the recent measurement of [28].

with the quantity on the left-hand side being the Hubble expansion rate, reciprocal to the expansion timescale τ_H discussed above. The total energy density ρ is the sum of all the energy densities present in the medium, and G_N is the Newton's constant. The energy density together with the total pressure density p satisfy the "energy conservation" law

$$a\frac{d\rho}{da} + 3(p + \rho) = 0. \tag{2.3}$$

At the temperatures of interest the dominant components of the plasma are photons γ, electrons and positrons $e^{\pm}$, three flavours of active neutrinos (ν_e, ν_μ, ν_τ) and sterile neutrinos.[4] Working with the particle kinematics in the expanding Universe it is convenient to use *conformal momentum y* instead of the usual physical momentum p. The two are related through $y = pa$. The quantitative description of the plasma population is provided by the distribution functions f_α, that are the numbers of particles α per "unit cell" of the phase space $d^3p\, d^3x = (2\pi)^3$. At keV–MeV temperatures the medium is homogeneous and the distribution functions are independent of spatial coordinates of particles, and due to isotropy they do not depend on the direction of the particle momentum. That simplifies the description of their evolution and therefore

$$\frac{df}{dt} \equiv \left(\frac{\partial f}{\partial t} - Hp\frac{\partial f}{\partial p}\right) = \frac{\partial f(t, y)}{\partial t} \tag{2.4}$$

holds. The goal is to find the distribution functions of all relevant particles and to use them to compute the energy density and pressure as a function of time and scale-factor, closing the system of eqs. (2.2)–(2.3) via

$$\rho = \sum_i \frac{g_i}{2\pi^2} \int f_i E_i p^2 dp\,; \quad p = \sum_i \frac{g_i}{6\pi^2} \int f_i \frac{p^4}{E_i} dp \tag{2.5}$$

Here the summation goes over all plasma particles, g_i, m_i is the number of degrees of freedom and mass of i-th particle respectively, $E_i = \sqrt{p^2 + m_i^2}$.

If interaction rate of the particles is much faster than the Hubble expansion rate, their distribution functions are given by either the Bose-Einstein, or the Fermi-Dirac distributions. This is the case for photons, electrons and positrons — that are kept in equilibrium due to intensive electromagnetic interactions

$$f_\gamma = \frac{1}{e^{E/T} - 1}\,, \quad f_e = \frac{1}{e^{E/T} + 1}. \tag{2.6}$$

Their contribution to the energy and pressure in eqs. (2.2), (2.3) is hence determined by the single parameter — temperature. However, to describe the contributions of the other particles one has to solve *kinetic* equations involving them (see sections 2.3–2.4 below).

2.2 Baryonic matter

The contribution of the baryonic matter to the evolution of the hot plasma of relativistic species is proportional to the so-called baryon-to-photon ratio $\eta_B = n_B/n_\gamma$. The measurements of relic radiation [2] yield $\eta_B = (6.19 \pm 0.15) \times 10^{-10}$. One can see that baryons are

---

[4]Muons may appear in plasma from the decays of the sterile neutrinos with $M_s > 106\,\text{MeV}$. See section 2.4 for details.

present in negligible amount, and do not influence the dynamics of the remaining medium. This allows to analyze our problem in two steps. At STEP I we omit baryonic species and study how the temperature of the plasma, the expansion factor and neutrino distributions evolve in time from temperatures of the order of 100 MeV, when sterile neutrinos typically start to go out of equilibrium,[5] down to $T_{\rm Fin} \simeq 10$ keV when nuclear fusion reactions have ended. At STEP II we use these results to determine the outcome of the nuclear reaction network against the background of evolving electromagnetic plasma (section 2.5).

2.3 Active neutrinos at MeV temperatures

Weak interactions are not able to maintain the thermal equilibrium of active neutrinos with the plasma during all the expansion period we consider. A simple comparison of the weak collision rate $G_F^2 T^5$ and $H(T)$ tells that neutrino maintain their equilibrium with the rest of the plasma down to temperatures $T_{\rm dec} \sim$ few MeV. The process of neutrinos going out of equilibrium is usually referred to as *neutrino decoupling*. Throughout the paper we assume that *no* large lepton asymmetry is present so that the number of neutrinos is equal to the number of antineutrinos.[6] At temperatures higher than $T_{\rm dec}$ the distribution is therefore given by the Fermi-Dirac one, while at lower temperatures we have to solve the set of three Boltzmann equations

$$\frac{df_{\nu_\alpha}}{dt} = I_\alpha, \quad \alpha = e, \mu, \tau \,. \tag{2.7}$$

The details of the interactions, such as particle collisions, are encoded in the so-called collision terms I_α. The terms are explicitly [33]

$$I_\alpha = \frac{1}{2E_\alpha} \sum_{\rm in,out} \int S|\mathcal{M}|^2 F[f](2\pi)^4 \delta^4(p_{\rm in} - p_{\rm out}) \prod_{i=2}^Q \frac{d^3 p_i}{(2\pi)^3 2E_i} \,. \tag{2.8}$$

The sum runs over all the possible initial states "in" involving ν_α (represented by a particle set ν_α, 2, 3, ..., K) and the final states "out" ($K+1$, ..., Q). Matrix element $\mathcal{M}$ corresponds to the probability of the transition "in"–"out" to occur and the delta-function ensures the conservation of 4-momentum $p_{\rm in} = p_{\rm out}$. Symmetrization factor S is equal to 1, except of the transitions involving identical particles either in initial or in a final state. Relevant matrix elements together with the symmetrization factors are listed in appendix B. The interaction rates are dependent on the population of the medium, and the functional $F[f]$ describes this. In case when all the incoming and outgoing particles are fermions,

$$F[f] = (1 - f_{\nu_\alpha}) \ldots (1 - f_K) f_{K+1} \ldots f_Q - f_{\nu_\alpha} \ldots f_K (1 - f_{K+1}) \ldots (1 - f_Q). \tag{2.9}$$

When some of particles are bosons, one has to replace $(1 - f_R)$ by $(1 + f_R)$ for every bosonic particle R.

A simple estimate (see appendix C) demonstrates that the rates of transitions between neutrinos of different flavours are much faster than weak reactions. We argue that this phenomenon can be approximately described by the following modification of the Boltzmann equations

$$\frac{df_{\nu_\alpha}}{dt} = \sum_\beta I_\beta P_{\beta\alpha}. \tag{2.10}$$

---

[5]The exact "freeze-out" temperature depends on the mixing angle.

[6]For the previous studies of the BBN outcomes *with* the large lepton asymmetry present see e.g. [17, 29–32].

Summation is carried out over three active flavours and expressions for $P_{\beta\alpha}$ are listed in appendix C (eqs. (C.4)).

2.4 The impact of sterile neutrinos

As already mentioned, sterile neutrinos interact much more feebly than active neutrinos do. Nevertheless, at some high temperature sterile neutrinos may enter thermal equilibrium. Whether this happens or not depends on the thermal history of the Universe before the onset of the synthesis.[7] Even if they were in thermal equilibrium at early times, sterile neutrinos then necessarily decouple at temperatures *higher* than those of active neutrino decoupling. If sterile neutrinos were light and stable (or very long-lived), they would be relativistic and propagate freely in the medium, yielding $N_{\text{eff}} \approx 3 + g_S$ together with active neutrinos (g_S is the number of sterile neutrinos). However, sterile neutrinos decay into active neutrinos and other particles. The energies of the decay products may be very different from the typical energies of plasma particles. For particles that equilibrate quickly (such as electrons or photons), this "injection" results in the fast redistribution of the energy between all particles in equilibrium and effectively the process looks like a temperature increase (more precisely, it just slows down the cooling of the Universe). But for particles that either are not in equilibrium or are about to fall out of it, such as active neutrinos at few MeV, the "injection" *modifies* the form of their spectra. The other mass-induced effect is that sterile neutrinos may switch from the relativistic regime (when their average momentum is larger than mass), that is established at large temperatures, to the non-relativistic one, due to the gravitational redshift.

For the quantitative description of sterile neutrino dynamics we utilize the Boltzmann equation similar to (2.7), replacing active neutrino everywhere therein by sterile neutrino ν_S

$$\frac{df_S}{dt} = I_S \,. \tag{2.11}$$

Reactions contributing to the right-hand side together with their probabilities are listed in tables 3–4 of appendix B. Note that we neglect the processes involving baryonic particles. However, they become important for temperatures near the QCD crossover temperature $T_{\text{QCD}} \simeq 200\,\text{MeV}$, when their density is not negligible anymore. More scattering channels of sterile neutrino would appear and their proper account is involved. However it seems to be reasonable to assert that the only modification the account will bring is to *lower* the decoupling temperature of sterile neutrinos.

Oscillation phenomenon does not affect significantly sterile neutrinos and therefore Boltzmann equation in its original form (2.11) is still valid, contrary to what we have found out for active neutrinos. An argument in favor of this statement is explained in appendix C.

When sterile neutrino is heavier than muon, the former particle can appear in the decay $\nu_S \to \mu^- + e^+ + \bar{\nu}_e$. However, the branching fraction of this decay mode does not even reach a percent for masses of sterile neutrino we consider (see e.g. [26]). Therefore we can neglect influence of both muons and other particles, appearing in the decay.

As a result we have six equations (2.2), (2.3), (2.10), and (2.11) describing primordial plasma at temperatures of interest. These equations contain six unknowns — scale factor $a(t)$, temperature $T(t)$ and four neutrino distribution functions, f_{ν_α} and f_S. The system of equations is therefore closed and we have solved it numerically at the STEP I.

---

[7]For example in the νMSM model at early times ($T \gg 100\,\text{GeV}$) initial densities of sterile neutrinos are negligible [34]. Then the neutrinos come into equilibrium at temperature T_+ (typically $T_+ = 10 \div 100\,\text{GeV}$) and freeze-out at temperatures $T_- \sim 0.5 - 5\,\text{GeV}$ [12].

2.5 Course of nuclear reactions

Outcome of the nuclear reaction chains is found numerically. For the Standard BBN model one of the earlier attempts was made with the code written by L. Kawano [35, 36]. However, the program in its original form is inappropriate for the account of the BSM physics, and we modified it for this work. Two technical remarks are in order here. First, we used the 1992 version of the program [36] as a starting point, and not the 1988 one, [35]. Therefore, the integration time steps were taken small enough, so that the integration procedure did not introduce an error, that was compensated as a shift in the resulting value of the Y_p,[8] the so-called "Kernan correction" [37]. Second, the code did not take into account the Coulomb and the nucleon finite-mass corrections to weak interaction rates, as well as radiative and finite-temperature effects.[9] We do not calculate directly these effects, but assume their net result to be in the form of the additive correction, which we took to be $\Delta Y_p = -0.0003$ [41]. The tests described in appendix A.1 demonstrate an agreement of thus modified "Kawano code" with the results of the other code, PArthENoPE [42], that takes a proper account of these effects.

Presence of sterile neutrinos alters the standard dynamics of the temperature and the expansion rate as well as the rates of weak interactions involving neutrons and protons. These quantities are known from the STEP I, so we have implemented the import of these data. Together with the change of ΔY_p indicated above, it has lead to the code, that became an essential tool of STEP II in our approach. The computations of nuclide evolution started from temperatures of several MeV, when the chemical equilibrium ceases to hold, up to temperatures T_{Fin}.

2.6 Adopted values of abundances of the light nuclei

The observables of the BBN are concentrations, or abundances, of light nuclides dispersed in the cosmos. The most relevant abundance in our problem is that of ^{4}He, as it is sensitive to the expansion rate of the Universe at MeV temperatures and neutrino distribution functions. The presence of sterile neutrinos in plasma typically increases the concentration of ^{4}He, described by Y_p. Accurate calculations carried out in the Standard Model [42] predict the values

$$Y_p^{\mathrm{SBBN}} = 0.2480 \qquad\qquad (\tau_n = 885.7 \text{ sec}) \qquad\qquad (2.12)$$

$$Y_p^{\mathrm{SBBN}} = 0.2465 \qquad\qquad (\tau_n = 878.5 \text{ sec}) \qquad\qquad (2.13)$$

depending on the lifetime of neutron, τ_n, see below.

There are two main methods of experimental determination of primordial Helium abundance. The first one is related to the studies of low-metallicity astrophysical environments and extrapolating them to zero metallicity case. The Y_p measurements are known to be dominated by systematic uncertainties. Therefore we adopt the Y_p values from the two most recent studies, refs. [1, 43] that have slightly different implications. For recent discussion of various systematic uncertainties in ^{4}He determination, see [44].

In ref. [1] the value $Y_p = 0.2565 \pm 0.0010(\mathrm{stat.}) \pm 0.0050(\mathrm{syst.})$ was obtained. Therefore, the 2σ intervals that we adopt in our studies are[10]

$$Y_p = 0.2495 - 0.2635 \quad (\text{ref. [1], } 2\sigma \text{ interval}) \qquad\qquad (2.14)$$

---

[8]We denote by Y_p the *mass fraction* of the ^{4}He, that is a fraction of the total baryon mass stored in the form of Helium-4

[9]For the accurate account of these corrections, see e.g. [4, 38–40].

[10]We add the systematic errors linearly.

One notices that this result is more than 2σ away from the Standard Model BBN predicted value of Y_p, eq. (2.12).

Using a subsample of the same data of [1], a different group had independently determined Y_p [43]. From their studies we adopt[11] $Y_p = 0.2574 \pm 0.0036(\text{stat.}) \pm 0.0050(\text{syst.})$. As a result,

$$Y_p = 0.2452 - 0.2696 \quad (\text{ref. [43], } 2\sigma \text{ interval}) \tag{2.15}$$

(this values of Y_p coincide with the Standard BBN one, (2.12), at about 1σ level).[12]

Second method of determination of Helium abundance is based on the CMB measurements. This method is believed to determine truly pristine value of Y_p, not prone to the systematics of astrophysical methods. However currently its uncertainties are still much larger than of the first method. The present measurements put it at

$$Y_p = 0.22 - 0.40, \quad N_{\text{eff}} = 3 \quad (\text{refs. [2, 46], } 2\sigma \text{ interval}) \tag{2.16}$$

again consistent with the Standard Model BBN at 1.5σ. Here N_{eff} is the so-called effective number of neutrino species

$$N_{\text{eff}} = \frac{120}{7\pi^2} \frac{\rho_{\nu_e} + \rho_{\nu_\mu} + \rho_{\nu_\tau}}{T^4}, \tag{2.17}$$

proportional to the ratio of the total energy, deposited into the active neutrino species to that of photons. Notice, that the bound (2.16) is based on assumption that before the onset of the recombination epoch the effective number of neutrino species is close to its SM value $N_{\text{eff}} \approx 3$. As we will see later, sterile neutrinos can significantly distort N_{eff}. For the values of N_{eff} strongly deviating from 3 the CMB bounds on Y_p gets modified. For example, the analysis carried out in [46] reveals that

$$Y_p = 0.10 - 0.33, \quad N_{\text{eff}} = 6 \quad (\text{ref. [46], } 2\sigma \text{ interval}). \tag{2.18}$$

The similar conclusion is reached if one employs the data of [47].

The other element produced during the BBN is the Deuterium, and recent observations determine its abundance to be

$$D/H = (2.2 - 3.5) \times 10^{-5} \quad (\text{ref. [4], } 3\sigma \text{ interval}). \tag{2.19}$$

This value is sensitive both to the baryon-to-photon ratio and to N_{eff}. In this work we adjust the value of baryon-to-photon ratio η at the beginning of the computation so that by $T_{\text{Fin}} \sim 10\,\text{keV}$ it is equal to the value given by cosmic microwave background measurements [2].

Finally, we mention another important uncertainty originating from the particle physics. There are two different measurements of neutron lifetime τ_n that are at tension with each other. Particle Data Group [27] provides $\tau_n = 885.7 \pm 0.8\,\text{sec}$, while measurements performed by Serebrov et al. [28] result in $\tau_n = 878.5 \pm 0.8\,\text{sec}$. We employ both results and explore the differences they lead to in what follows.

---

[11]We use the average value over metallicities, $\langle Y_p \rangle$ (eq. (8.2) of [43]) and leave the systematic error from [1].

[12]A study of [45], based on the independent dataset, provides the value $Y_p = 0.2477 \pm 0.0029$. Its upper bound becomes very close to that of (2.15) if one employs an additional systematic uncertainty at the level $\Delta Y_{\text{syst}} = 0.010$ (twice the value of systematic uncertainty of [1]).
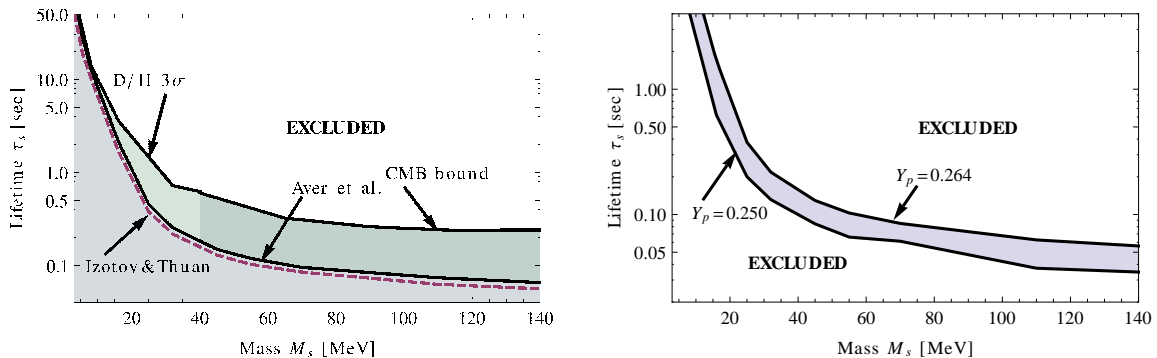
(a) 2σ upper bounds on sterile neutrino lifetime, based on different measurements of Y_p: ref. [1] ("Izotov & Thuan"); ref. [43] ("Aver et al."); refs. [2, 46] ("CMB bound").

(b) Upper *and lower* bounds on sterile neutrino lifetime, based on the measurements of [1]. The upper curve is the same as the dashed curve in the left panel.

Figure 2. Bounds (at 2σ level) on sterile neutrino lifetime as a function of their mass for various measurements of Y_p (summarized in section 2.6). All results are for mixing of sterile neutrino with electron flavour only (the dependence on the particular mixing patter is very weak, see below). For the CMB bound, we present only the result for masses $M_s > 40$ MeV where $N_{\rm eff} \approx 3$. For smaller masses we plot instead bounds based on 3σ Deuterium upper bound (2.19). For details, see section 3 and figure 3.

3   Results

In this section we present our main results: the bounds on sterile neutrino lifetime as a function of their masses and mixing patterns, as well as the bounds on the mixing angles. As discussed in the previous section, there are several systematic uncertainties in the determination of the ^{4}He abundance and therefore the results will depend on the adopted values of Y_p (together with the neutron lifetime, τ_n). We summarize these systematic effects below.

We start with comparing the upper bounds on sterile neutrino lifetime for different values of Y_p (see section 2.6). The figure 2a shows that the bounds from the two recent works [1, 43] are quite similar (the difference is of the order of 30%). The bound, based on [45] would give a result, similar to [43] as discussed above.

For the CMB bound in figure 2a, we present only the results for masses $M_s > 40$ MeV where $N_{\rm eff}$ does not deviate significantly from 3. Figure 3 indicates that for smaller masses the number of effective neutrino species increases significantly. It in turn affects the CMB helium bounds (cf. eqs. (2.16) and (2.17)). The accurate account of this effect goes beyond the scope of this work and we choose instead to plot stronger deuterium-based bounds (those of figure 3) in figure 2a for $M_s \lesssim 40$ MeV.

The lower bound on Y_p from the recent work of [1] is above the Standard BBN value (2.12) at $\sim 2\sigma$ level (see however [44]). The presence of sterile neutrinos in plasma of course relaxes this tension and therefore at 2σ the adopted values of Y_p (eq. (2.14)) provide both upper and *lower* bounds on sterile neutrino lifetime. This is shown in figure 2, right panel. At 3σ level the measurements of [1] are consistent with Standard BBN and the lower bound disappears.

Figure 3 shows the changes in Deuterium abundance and in the effective number of neutrino species, caused by sterile neutrinos (with parameters corresponding to the upper bound based on [1]). For these values of parameters the abundance lies within the 3σ bound-
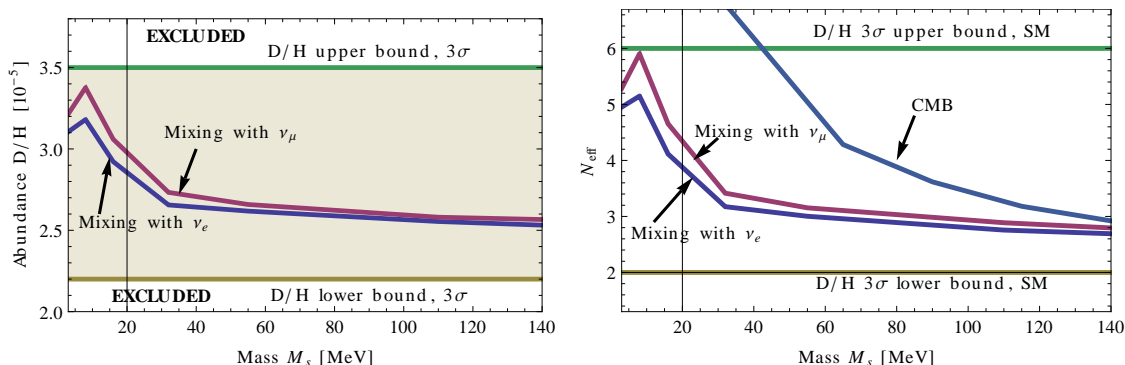
Figure 3. *Left:* deuterium abundance, with the shaded region corresponding to the *allowed* 3σ range, based on [4]. *Right:* effective number of neutrino species (the ratio of the effective neutrino temperature to the photon temperature at $T \sim$ few keV) as a result of decay of sterile neutrino. The horizontal "SM" lines indicate $N_{\rm eff}$ that corresponds to the boundary of the 3σ range [4], in the SM with the number of relativistic species deviating from $N_{\rm eff} \approx 3$. In both panels, parameters of sterile neutrinos correspond to the upper bound on Y_p from [1] (see eq. (2.14)), except of the "CMB" line that corresponds to the upper bound from [2, 46] (see eq. (2.16)).

aries (2.19). And for the highest effective number of neutrinos reached, $N_{\rm eff} = 6$, D/H is close to the 3σ upper bound. Notice that the same relation between $N_{\rm eff}$ and D/H is observed in the model without new particles but with the effective number of neutrinos different from 3. The effective number of neutrino species does not define the Helium abundance though. Otherwise the same Y_p bound [1] would predict *only one particular* value of $N_{\rm eff}$, which is not case, as the inspection of figure 3 shows.

The influence of another systematic uncertainty (the lifetime of neutron, τ_n) is negligible. Indeed, the relative difference between sterile neutrino lifetimes were found to be of the order of 5% for two choices of τ_n — from [28] and from [27] (taking the same Y_p bound from [43]).

Next we investigate the dependence of the resulting bounds on the mixing patterns of sterile neutrinos. Naively, one would expect that sterile neutrinos mixing "only with ν_e" and "only with ν_μ" should have different effect of Y_p. However, it is the energy "injection" rate (i.e. the overall decay rate of sterile neutrinos) that is *more important* for the dynamics of plasma before the onset of nucleosynthesis. This quantity depends on the lifetime τ_s and the mass M_s of the neutrino. Mixing patterns affect mostly the concentration of particular decay products, but not the injection rate. In addition, the neutrino oscillations (fast at the BBN epoch) make the difference between flavours less pronounced (see appendix C). As a result, mixing patterns give essentially the same results with the difference at the level of tens of per cent (see figures 4, 5).

4 Discussion

In this work we considered the influence of decaying particles with the masses few MeV – 140 MeV on the primordial abundance of light elements (D and ^{4}He). Such particles appear in many cosmological scenarios [12, 13, 18–23, 48–50]. Particularly, we concentrated on the properties of sterile neutrinos and derived constraints on their lifetime imposed by the present measurements of primordial Helium abundance Y_p. Sterile neutrinos are super-weakly interacting particles, quadratically mixed with the active flavours.
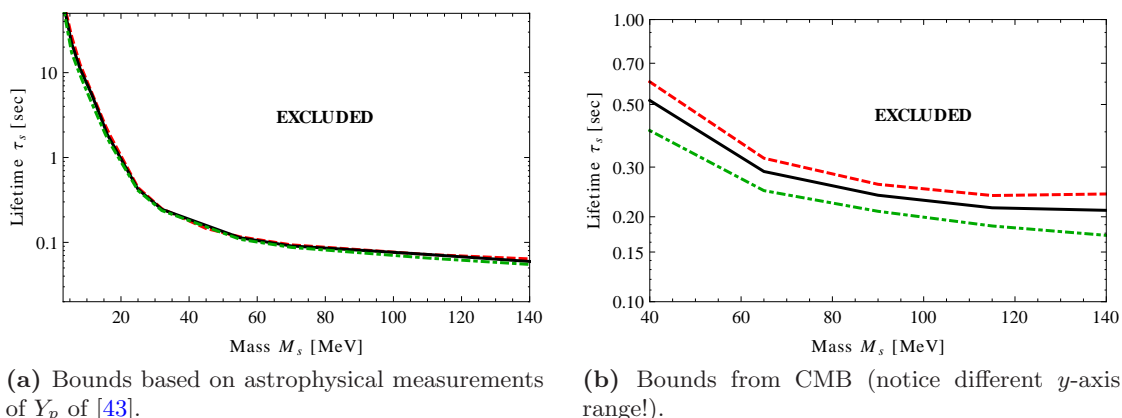
(a) Bounds based on astrophysical measurements of Y_p of [43].

(b) Bounds from CMB (notice different y-axis range!).

Figure 4. Upper bound for sterile neutrino lifetime for different mixing patterns: mixing with ν_e-only (red dashed line), ν_μ-only (green dashed-dotted line) and equal mixing with ν_e and ν_μ flavours (black solid line). All bounds are derived for the lifetime of neutron τ_n adopted from [27]. The effect of different mixing patterns is at the level $\sim 10-50\%$ and can only be seen in the right panel because of the different y axis. In the right panel, only the masses $M_s > 40$ MeV are presented. For details, see section 3 and figure 3.
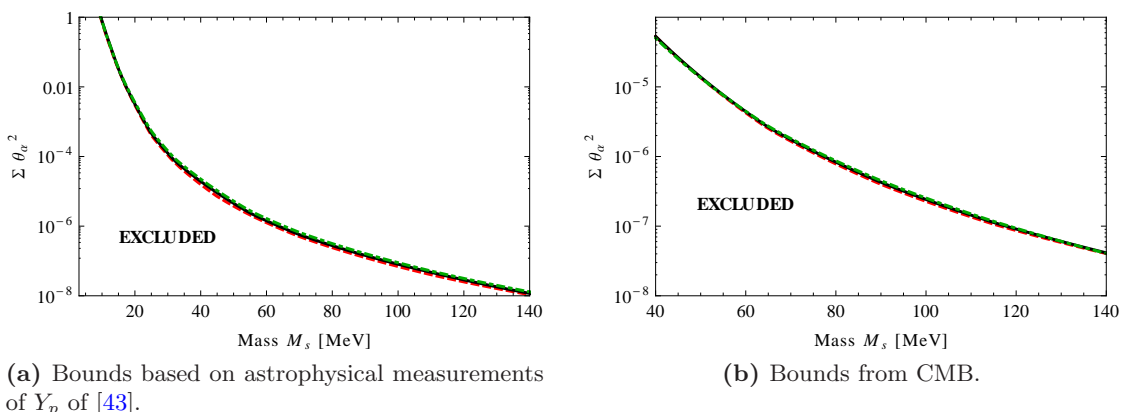

(a) Bounds based on astrophysical measurements of Y_p of [43].

(b) Bounds from CMB.

Figure 5. *Lower* bound on mixing angles of sterile neutrinos for different mixing patterns: mixing with ν_e-only (red dashed line), ν_μ-only (green dashed-dotted line) and equal mixing with ν_e and ν_μ flavours (black solid line). Both types of bounds are derived by assuming lifetime of the neutron τ_n from [27]. In the right panel, only the masses $M_s > 40$ MeV are presented. For details, see section 3 and figure 3.

We analyzed the case of one Majorana sterile neutrino with 4 degrees of freedom (if sterile neutrinos were kept in thermal equilibrium it would be equivalent to $g_s = 2$ species of active neutrinos). Since the plasma evolution is mostly affected by the overall decay rate of sterile neutrinos, the lifetime bounds that we obtained are essentially independent of the particular mixing patterns, as figures 4, 5 demonstrate.

In the paper [16] a similar model was considered with one *Dirac* sterile neutrino. Dirac sterile neutrino has the same 4 degrees of freedom and influences primordial plasma in the same way (if it has the same spectrum, lifetime and mixing pattern). However, in [16] effect of active-neutrino oscillations was not taken into account, and some simplifying approximations
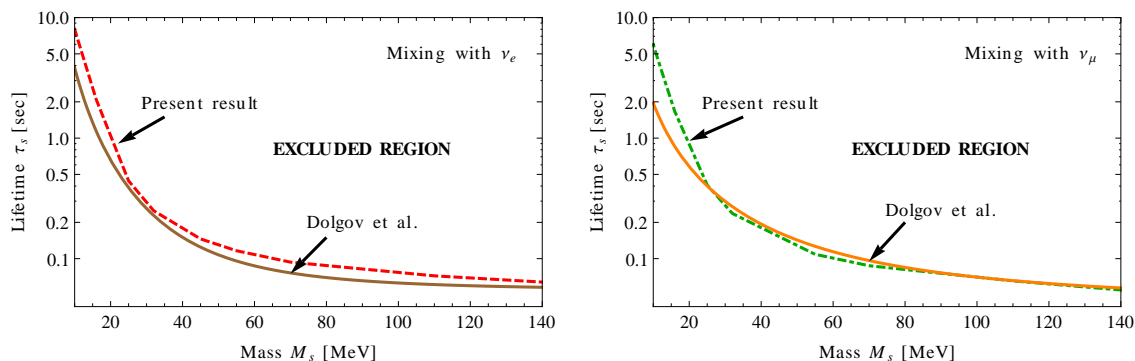
Figure 6. Comparison with the previous results of [15, 16].

like Boltzmann statistics were employed. To provide corresponding analysis we wrote code that solves more accurate Boltzmann equations describing kinetics of neutrino than what were used in [16]. We compare the results of this work with the previous bounds [15, 16] in figure 6. We see that our results are broadly consistent with the previous works. The differences for a given mixing pattern of sterile neutrinos can be as large as a factor of 2.5 for some masses.

The presence of sterile neutrinos in the plasma affects the effective number of neutrino degrees of freedom, N_{eff}. Figure 3, right panel shows that N_{eff} between 2.7 and 6 are possible for different mixing angles and masses, which could explain a larger than 3 values of N_{eff}, reported recently in several CMB observations (see e.g. [46, 47, 51], but also [52]).

Decaying sterile neutrinos with the masses $100 - 500\,\text{MeV}$ and lifetimes from seconds to minutes and their influence on N_{eff} and entropy production have been recently considered in [18] (see also [53]) where it was demonstrated that they can lead to $N_{\text{eff}} \neq 3$ and can therefore be probed with the CMB measurements. The results of the present work demonstrate that in the region $100 - 140\,\text{MeV}$ where we overlap with the parameter space, studied in [18], the primordial nucleosynthesis restricts the lifetime of sterile neutrinos to be well below $1\,\text{sec}$ (see figure 2, left panel).

Finally, it is interesting to compare the upper bound on sterile neutrino lifetime, derived in this paper with the *lower bounds* that come from direct experimental searches for sterile neutrinos (see [26, 54, 55]). These latter bounds are based on the assumption that sterile neutrinos with four degrees of freedom are solely responsible for the observed pattern of neutrino oscillations via the see-saw mechanism [55]. The appropriate comparison, based on [55], is presented in figure 7. No allowed values of sterile neutrino lifetimes for $1\,\text{MeV} \lesssim M_s < 140\,\text{MeV}$ exist for either type of neutrino mass hierarchy (i.e. the upper bound is *smaller* than the lower bound, see the purple double-shaded region in figure 7). Notice, that if the astrophysical bounds on Helium [1, 43] were used for $M_s \gtrsim 40\,\text{MeV}$ in figure 7, instead of the CMB bound, the resulting lifetime bounds would become stronger (by as much as a factor of 4) in this mass range. *We stress that for this conclusion it is essential* that MeV sterile neutrinos are responsible for neutrino oscillations. For example, a model in which sterile neutrinos couple to ν_τ *only* (and therefore do not contribute to the mixing between active neutrino flavours), *is allowed* even if one confronts the strongest BBN bounds (based on the astrophysical Helium measurements) with the direct accelerator bounds, see figure 8 for details.
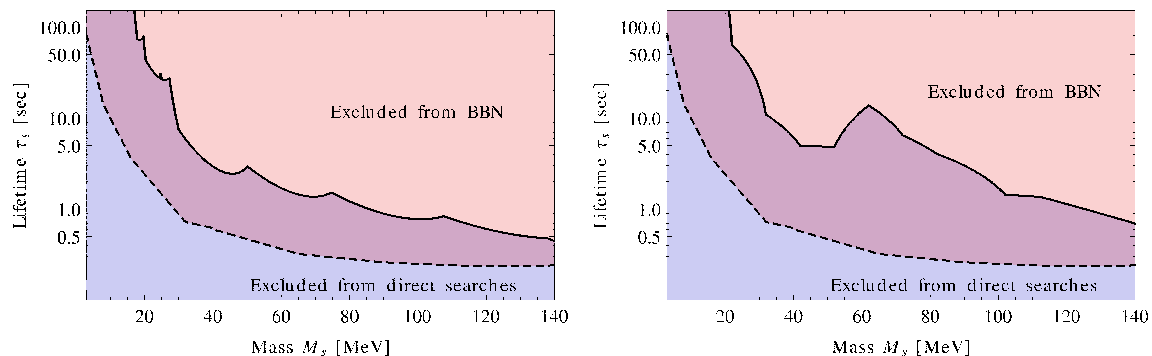
Figure 7. Experimental 3σ *lower* bounds on the lifetime of sterile neutrinos [55] (solid line), combined with the *upper* bounds from this work (dashed line), corresponding to the *weakest* bound in figure 2a. The accelerator bounds are for two Majorana sterile neutrinos solely responsible for neutrino oscillations. *Left:* normal hierarchy, *right:* inverted hierarchy. Combination of BBN bounds with direct experimental searches demonstrates that sterile neutrinos with the masses in 1–140 MeV range, solely responsible for neutrino oscillations are ruled out. See sections 3, 4 for details.
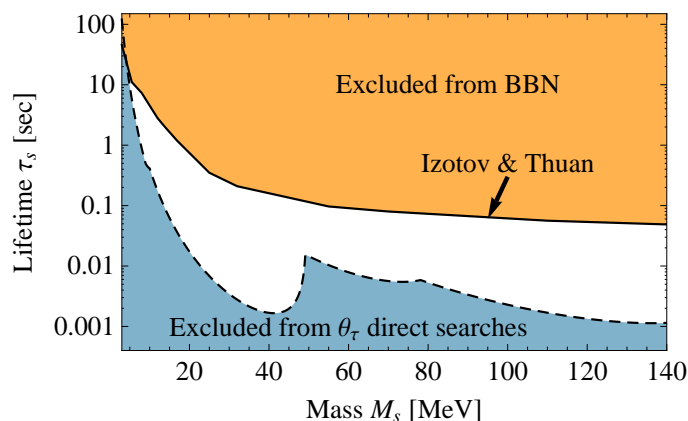

Figure 8. Comparison of direct accelerator constraints and BBN bounds, based on the Helium-4 measurements of [1] in the model where sterile neutrinos mix with ν_τ *only*. Unlike the case, presented in figure 7 there is an allowed region of parameter space for most of the masses below 140 MeV.

Acknowledgments

---

[13]http://sec.bitp.kiev.ua.

[14]http://virgo.org.ua.

Code	Y_p for τ_n from PDG [27]	Y_p for τ_n from [28]
(Modified) Kawano code [36]	0.2472	0.2457
PArthENoPE code [42]	0.2480	0.2465
Difference	-0.0008	-0.0008

Table 1. Values of Helium abundance Y_p in the Standard Model BBN (SBBN) and their dependence on the neutron lifetime, τ_n.

A Tests of the numerical approach

The section below summarizes the comparison of the present work with the previous ones that analyzed the influence of the MeV particles on primordial nucleosynthesis. Throughout this section, we normalize scale factor by imposing condition $aT = 1$ at the initial moment. Conformal momentum is $y = pa$ with the same normalization of the scale factor. In the figures that contain both the solid and the dashed curves, the former correspond to the results obtained with our code, and the latter — to the original results of the other papers.

A.1 Standard Model BBN

First we considered the nucleosynthesis in Universe filled with the Standard Model particles only. We compute the actual *non-equilibrium* form of the active neutrino spectra during their decoupling. The results of the present work are compared with those of [24, 25, 57]. In [24, 25] neutrino oscillations were neglected, while in [57] the effect was taken into account. Figure 9 shows the evolution of the quantity aT as a function of temperature. It is identical to the figure 1 in ref. [25]. Figures 10, 11 show how distorted neutrino spectra f_{ν_α} are, compared to the thermal distribution $f^{\rm eq} = (e^y + 1)^{-1}$. One can see good agreement between the results. We believe that the difference, that is present nevertheless, arises solely due to our one-step time integration method of the stiff kinetic equations, that is not as accurate as the method employed in refs. [24, 57].

We turned off flavour oscillations and compared asymptotic values of ratio aT at low temperatures together with the effective number of neutrino species, $N_{\rm eff}$. For the former quantity, refs. [24, 57] present values 1.3991 and 1.3990, respectively. On the other hand, we derived 1.3996. For the number of neutrino species in absence of neutrino oscillations, the same refs. [24, 57] provide numbers 3.034 and 3.035, respectively, while we get 3.028.[15]

The resulting Y_p is summarized in table 1 for different values of neutron lifetime τ_n. We also provide a comparison of the modified version of the Kawano code [36] that we adopted for computing nuclear reactions with a newer code, PArthENoPE [42]. By comparing the results of PArthENoPE and the modified KAWANO code, we find the former to be larger by 0.0008 than the latter. We use the shift $\Delta Y_p = -0.0008$ as a correction in our subsequent results.

A.2 Test of energy conservation

If all weak reactions involving electrons and positrons are turned off, neutrinos decouple from the rest of plasma. Then the energy conservation law (2.3) holds *separately* for the neutrino component and for the remaining particles. In approximation of zero mass of electron

---

[15]Ref. [57] the takes into account both the effects of neutrino oscillations and QED corrections, the latter changes the result significantly. As a result we could not compare the effect of *neutrino oscillations only*.
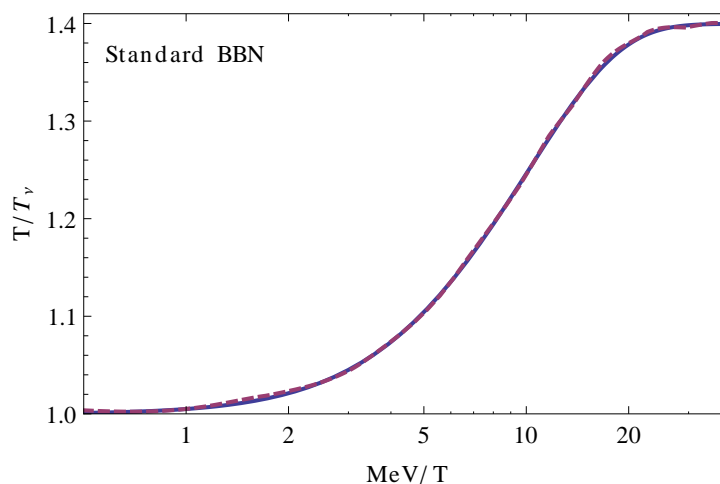
Figure 9. T/T_ν as a function of inverse temperature T^{-1}. The *solid* line is produced by the code of the present work, the *dashed* — the result of [25].
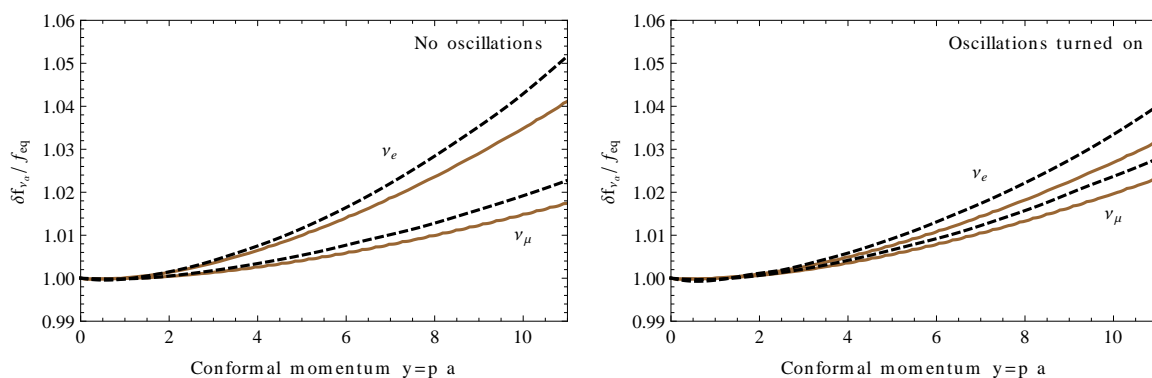

Figure 10. Relative distortions of neutrino spectra before the onset of BBN. *Left:* neutrino flavour oscillations are neglected, *right:* the oscillations are taken into account, with the parameter choice $\theta_{13} = 0$, $\sin^2 \theta_{23} = 0.5$, $\sin^2 \theta_{12} = 0.3$ used in [57]. In both panels, the pair of upper curves shows the distortion of the electron neutrino, the lower — of ν_μ. In each pair, the solid curve is the result of this work, and the dashed is from figure 2 of [57].

we obtain

$$\frac{d(aT)}{dt} = 0 \tag{A.1}$$

similar to eq. (A.3). As a corollary, product aT is conserved. On the other hand, our code solves the equation (2.3) involving *all* medium components simultaneously. And it turns out that the relation (A.1) is not a trivial consequence of the numerical computation. Therefore the check of the conservation serves as a test of the code. We considered separately scattering and decay processes involving neutrinos and observed conservation of aT with precision of order 0.2%.
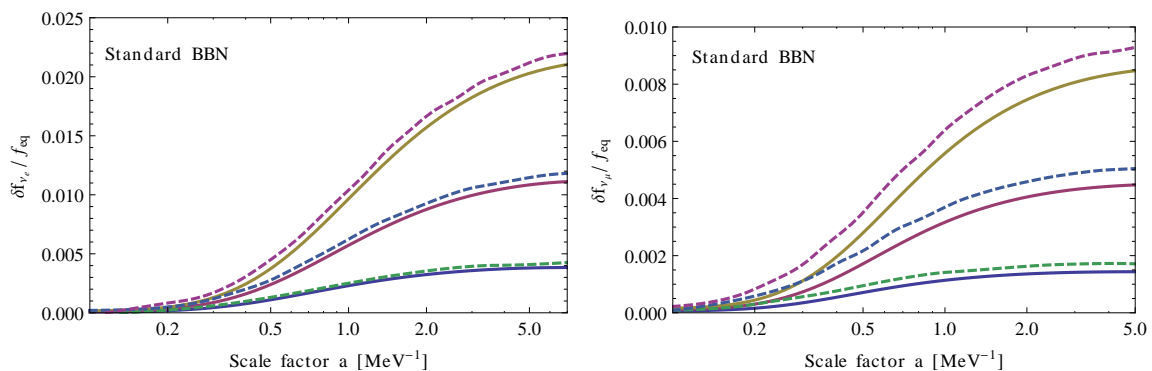
Figure 11. *Left:* relative distortion of ν_e spectra $\delta f_{\nu_e}/f_{eq}$ for conformal momenta $y = 3, 5, 7$ (from bottom to up). *Right:* the same, but for muon neutrino. In each pair of curves the solid one corresponds to this work and the dashed one is from [25].
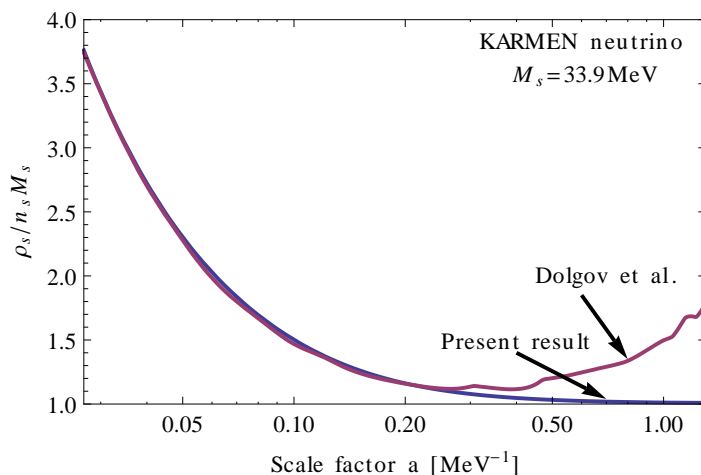

Figure 12. Ratio $\rho_s/n_s M_s$ as a function of scale factor for $M_s = 33.9$ MeV sterile neutrino. The upper curve is the result of ref. [15], the lower curve is the present work.

A.3 Heavy sterile Dirac neutrino

Next we have tested model with *one* sterile *Dirac* neutrino ν_S with mass $M_s = 33.9$ MeV, mixed with ν_τ [15]. This neutrino was assumed to be in thermal equilibrium with plasma at $T \gtrsim 50$ MeV. To simplify the problem, the authors of [15] used the *Boltzmann equilibrium* statistics for active species in collision integral for a sterile neutrino.

Being in equilibrium the sterile neutrino spectrum becomes more and more non-relativistic with time due to the redshift. Therefore the ratio $\rho_s/M_s n_s$ of the energy density ρ_s to the mass times number density n_s should approach 1 at lower temperatures. We have recomputed the evolution of the system using our code, without the Boltzmann approximation. Figure 12 shows the comparison of the results with those of [15] for sterile neutrino lifetime $\tau_s = 0.3$ sec. Both results coincide till $T \approx 5$ MeV and after that moment ratio $\rho_s/M_s n_s$ of [15] stops decreasing, while the numerical result we obtained shows the expected behaviour — the ratio continues to decrease, approaching 1.
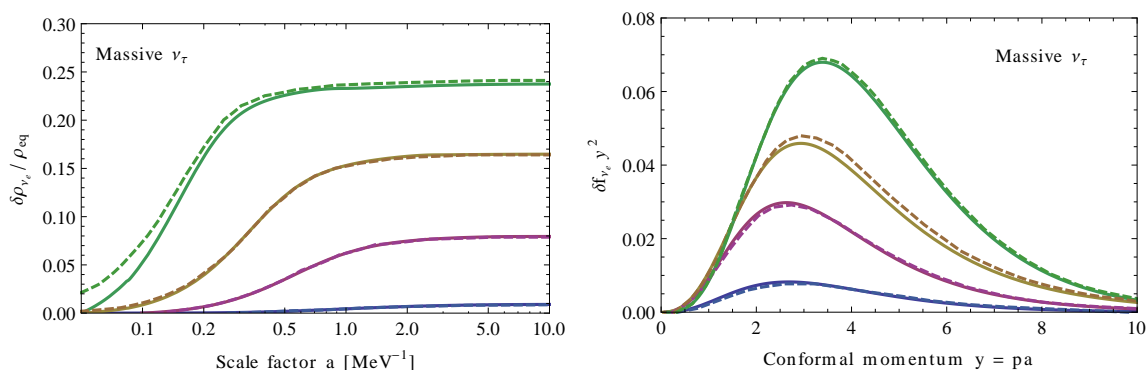
Figure 13. *Left:* relative deviation from its equilibrium value of ν_e energy density $\delta\rho_{\nu_e}/\rho_{\rm eq}$ in a model where tau neutrino is massive. *Right:* spectrum distortion $y^2\delta f_{\nu_e}/f_{\rm eq}$ for the same model. In both panels $M_{\nu_\tau} = 0, 3, 7, 20$ MeV from bottom to top, the solid curves depict the numerical results of this work, and the dashed — the results of [19].

A.4 Massive ν_τ

Next we considered a model with the massive tau neutrino [19, 21]. Figure 13 presents relative deviation of the energy densities of massless neutrinos $\delta\rho_\nu/\rho_{\rm eq}$ produced by our code and plotted in [19]. $\rho_{\rm eq} = \frac{7\pi^2 T^4}{120}$ is the equilibrium energy density of one neutrino specie, and $\delta\rho_\nu = \rho_\nu - \rho_\nu^{\rm eq}$. In figure 13 distortion of electron neutrino spectrum $y^2\delta f_{\nu_e}/f_{\rm eq}$ is depicted. Here one observes good agreement between the results.

A.5 Late reheating model

To test the treatment of MeV decaying particles, we considered the low-reheating models with the reheating temperature of several MeV [22, 23]. In [22] heavy non-relativistic particles were considered, that dominated the energy density of the Universe once and then decayed into electrons, positrons or photons (so that decay products are quickly thermalized). The most important output is the effective number of active neutrino species $N_{\rm eff}$ (defined in eq. (2.17)). Dependence of this quantity on decay width of heavy particle is presented in figure 14. We have noticed some difference between the results of cited papers and those of our code. We believe that this is due to the different approximations made. For example, in both works [22, 23] the scattering processes involving only neutrinos were not taken into account, approximation of Boltzmann statistics was used throughout and electron mass was neglected. We checked that the account of finite electron mass gives a gain of 5% to the $N_{\rm eff}$ for $\tau = 0.1$s, while the account of scatterings involving only neutrinos gives rise of 1%.

A.6 Instant thermalization of decay products

Next we considered a model with two heavy Majorana sterile neutrinos, similar to the νMSM. However, we assumed that for any mass of sterile neutrino it can decay *only* via channels listed in table 4 of appendix B. It is not a natural assumption, because usually sterile neutrinos heavier than pion decay dominantly into states containing mesons [26]. Also we approximated sterile neutrino spectrum as a non-relativistic one, while all the other particles are relativistic and in equilibrium all the time. In this case the system may be adequately described by the kinetic equation

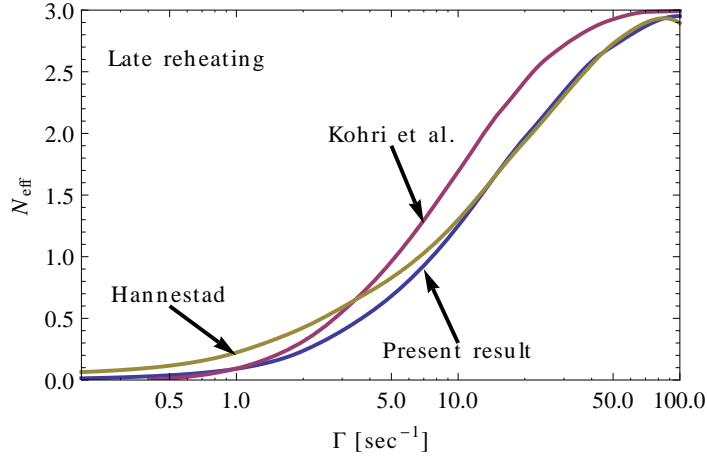$$\frac{d\rho_s}{dt} + 3\frac{\dot{a}}{a}\rho_s = -\Gamma_s\rho_s \tag{A.2}$$

Figure 14. Effective number of neutrino species N_{eff} depending on decay width of heavy non-relativistic particles. Comparison of the results of this work and refs. [22, 23].
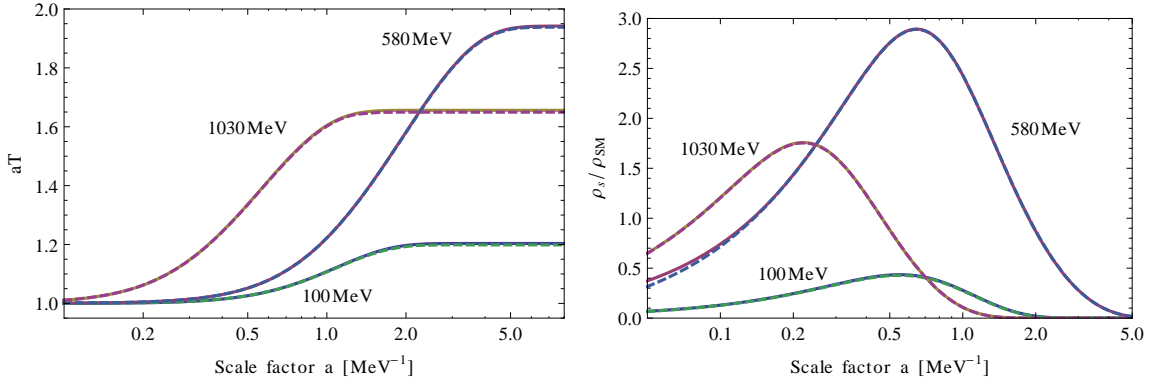

Figure 15. *Left:* evolution of aT for the model of section A.6. *Right:* ρ_s/ρ_{SM}. We consider three parameter sets: sterile neutrino mass $M_s = 580\,\text{MeV}$ with lifetime $\tau = 1\text{sec}$; $M_s = 1030\,\text{MeV}$ with $\tau = 0.1\text{sec}$; $M_s = 100\text{MeV}$, $\tau = 0.5\text{sec}$. The solid line depicts the numerical result of this work, dashed — the semianalytical calculation.

together with the Friedmann equations (2.2)–(2.3). The latter of these equations can be rewritten as

$$\frac{d(aT)}{dt} = \frac{30a\Gamma_s\rho_s}{43\pi^2T^3} \tag{A.3}$$

Γ_s is the decay width of sterile neutrino, ρ_s is the energy density of sterile neutrinos, and we have used expression for the energy and pressure densities of relativistic species $\rho_{\text{rel}} = 3p_{\text{rel}} = 43\pi^2T^4/120$.

In figures 15 the evolution of quantities aT and ρ_s/ρ_{rel} is compared between the results of our code and the semi-analytic integration of eqs. (A.2)–(A.3) for three different sets of masses and lifetimes. One can see very good agreement between these results, maximum relative deviation is 1%.

Process $(1 + 2 \rightarrow 3 + 4)$	S	$SG_F^{-2} |\mathcal{M}|^2$
$\nu_\alpha + \nu_\beta \rightarrow \nu_\alpha + \nu_\beta$	1	$32(p_1 \cdot p_2)(p_3 \cdot p_4)$
$\nu_\alpha + \bar{\nu}_\beta \rightarrow \nu_\alpha + \bar{\nu}_\beta$	1	$32(p_1 \cdot p_4)(p_2 \cdot p_3)$
$\nu_\alpha + \nu_\alpha \rightarrow \nu_\alpha + \nu_\alpha$	1/2	$64(p_1 \cdot p_2)(p_3 \cdot p_4)$
$\nu_\alpha + \bar{\nu}_\alpha \rightarrow \nu_\alpha + \bar{\nu}_\alpha$	1	$128(p_1 \cdot p_4)(p_2 \cdot p_3)$
$\nu_\alpha + \bar{\nu}_\alpha \rightarrow \nu_\beta + \bar{\nu}_\beta$	1	$32(p_1 \cdot p_4)(p_2 \cdot p_3)$
$\nu_e + \bar{\nu}_e \rightarrow e^+ + e^-$	1	$128[g_L^2(p_1 \cdot p_4)(p_2 \cdot p_3)+$
		$g_R^2(p_1 \cdot p_3)(p_2 \cdot p_4) + g_L g_R m_e^2(p_1 \cdot p_2)]$
$\nu_e + e^- \rightarrow \nu_e + e^-$	1	$128[g_L^2(p_1 \cdot p_2)(p_3 \cdot p_4)+$
		$g_R^2(p_1 \cdot p_4)(p_2 \cdot p_3) - g_L g_R m_e^2(p_1 \cdot p_3)]$
$\nu_e + e^+ \rightarrow \nu_e + e^+$	1	$128[g_L^2(p_1 \cdot p_4)(p_2 \cdot p_3)+$
		$g_R^2(p_1 \cdot p_2)(p_3 \cdot p_4) - g_L g_R m_e^2(p_1 \cdot p_3)]$
$\nu_{\mu(\tau)} + \bar{\nu}_{\mu(\tau)} \rightarrow e^+ + e^-$	1	$128[\tilde{g}_L^2(p_1 \cdot p_4)(p_2 \cdot p_3)+$
		$g_R^2(p_1 \cdot p_3)(p_2 \cdot p_4) + \tilde{g}_L g_R m_e^2(p_1 \cdot p_2)]$
$\nu_{\mu(\tau)} + e^- \rightarrow \nu_{\mu(\tau)} + e^-$	1	$128[\tilde{g}_L^2(p_1 \cdot p_2)(p_3 \cdot p_4)+$
		$g_R^2(p_1 \cdot p_4)(p_2 \cdot p_3) - \tilde{g}_L g_R m_e^2(p_1 \cdot p_3)]$
$\nu_{\mu(\tau)} + e^+ \rightarrow \nu_{\mu(\tau)} + e^+$	1	$128[\tilde{g}_L^2(p_1 \cdot p_4)(p_2 \cdot p_3)+$
		$g_R^2(p_1 \cdot p_2)(p_3 \cdot p_4) - \tilde{g}_L g_R m_e^2(p_1 \cdot p_3)]$

Table 2. Squared matrix elements for weak processes involving active species only. S is the symmetrization factor; $\alpha, \beta = e, \mu, \tau$. In all processes we take $\alpha \neq \beta$. The results coincide with those of ref. [25].

B Tree-level matrix elements

In this appendix we summarize the matrix elements we used for computing the collision integrals in Boltzmann equation. The squares of the matrix elements for Standard Model particles only are listed in table 2, while the squares of the matrix elements of processes with sterile neutrinos are summarized in tables 3, 4. In these expressions, averaging over helicities of incoming particles and summation over those of outgoing products is assumed. The reactions are considered for two cases. In the first one sterile neutrino is a right-chiral Majorana neutrino that has 2 helicity degrees of freedom. That is actually the case in our problem, where we have two neutrinos f this kind. The other case corresponds to sterile neutrino of Dirac nature. Dirac fermions have both right- and left-chiral components, hence yielding 4 degrees of freedom in total. Expressions listed in tables 3, 4 are applicable for both cases of the neutrino nature. Moreover, to complete the list of possible tree-level reactions, one has to consider charge-conjugated channels and take into account that Dirac particle is distinct from its antiparticle, while Majorana neutrino is not.

Throughout this section we use the notations $g_R = \sin^2\theta_W$, $g_L = 1/2 + \sin^2\theta_W$, $\tilde{g}_L = -1/2 + \sin^2\theta_W$, where θ_W is the Weinberg angle so that $\sin^2\theta_W \approx 0.23$. The resulting expressions coincide with [15, 25].

Process $(1 + 2 \rightarrow 3 + 4)$	S	$SG_F^{-2}\,\lvert\mathcal{M}\rvert^2$
$\nu_s + \nu_\beta \rightarrow \nu_\alpha + \nu_\beta$	1	$32\vartheta_\alpha^2(p_1 \cdot p_2)(p_3 \cdot p_4)$
$\nu_s + \bar{\nu}_\beta \rightarrow \nu_\alpha + \bar{\nu}_\beta$	1	$32\vartheta_\alpha^2(p_1 \cdot p_4)(p_2 \cdot p_3)$
$\nu_s + \nu_\alpha \rightarrow \nu_\alpha + \nu_\alpha$	$1/2$	$64\vartheta_\alpha^2(p_1 \cdot p_2)(p_3 \cdot p_4)$
$\nu_s + \bar{\nu}_\alpha \rightarrow \nu_\alpha + \bar{\nu}_\alpha$	1	$128\vartheta_\alpha^2(p_1 \cdot p_4)(p_2 \cdot p_3)$
$\nu_s + \bar{\nu}_\alpha \rightarrow \nu_\beta + \bar{\nu}_\beta$	1	$32\vartheta_\alpha^2(p_1 \cdot p_4)(p_2 \cdot p_3)$
$\nu_s + \bar{\nu}_e \rightarrow e^+ + e^-$	1	$128\vartheta_e^2[g_L^2(p_1 \cdot p_4)(p_2 \cdot p_3)+$ $g_R^2(p_1 \cdot p_3)(p_2 \cdot p_4) + g_L g_R m_e^2(p_1 \cdot p_2)]$
$\nu_s + e^- \rightarrow \nu_e + e^-$	1	$128\vartheta_e^2[g_L^2(p_1 \cdot p_2)(p_3 \cdot p_4)+$ $g_R^2(p_1 \cdot p_4)(p_2 \cdot p_3) - g_L g_R m_e^2(p_1 \cdot p_3)]$
$\nu_s + e^+ \rightarrow \nu_e + e^+$	1	$128\vartheta_e^2[g_L^2(p_1 \cdot p_4)(p_2 \cdot p_3)+$ $g_R^2(p_1 \cdot p_2)(p_3 \cdot p_4) - g_L g_R m_e^2(p_1 \cdot p_3)]$
$\nu_s + \bar{\nu}_{\mu(\tau)} \rightarrow e^+ + e^-$	1	$128\vartheta_{\mu(\tau)}^2[\tilde{g}_L^2(p_1 \cdot p_4)(p_2 \cdot p_3)+$ $g_R^2(p_1 \cdot p_3)(p_2 \cdot p_4) + \tilde{g}_L g_R m_e^2(p_1 \cdot p_2)]$
$\nu_s + e^- \rightarrow \nu_{\mu(\tau)} + e^-$	1	$128\vartheta_{\mu(\tau)}^2[\tilde{g}_L^2(p_1 \cdot p_2)(p_3 \cdot p_4)+$ $g_R^2(p_1 \cdot p_4)(p_2 \cdot p_3) - \tilde{g}_L g_R m_e^2(p_1 \cdot p_3)]$
$\nu_s + e^+ \rightarrow \nu_{\mu(\tau)} + e^+$	1	$128\vartheta_{\mu(\tau)}^2[\tilde{g}_L^2(p_1 \cdot p_4)(p_2 \cdot p_3)+$ $g_R^2(p_1 \cdot p_2)(p_3 \cdot p_4) - \tilde{g}_L g_R m_e^2(p_1 \cdot p_3)]$

Table 3. Squared matrix elements for *scatterings* of sterile neutrinos ν_S. Here S is the symmetrization factor; $\alpha, \beta = e, \mu, \tau$; $\alpha \neq \beta$. ϑ_α is the mixing angle of sterile neutrino with ν_α. The results are applicable for one right-chiral Majorana neutrino as well as for one Dirac neutrino, for details see text.

Process $(1 \rightarrow 2 + 3 + 4)$	S	$SG_F^{-2}\,\lvert\mathcal{M}\rvert^2$
$\nu_S \rightarrow \nu_\alpha + \nu_\beta + \bar{\nu}_\beta$	1	$32\,\vartheta_\alpha^2(p_1 \cdot p_4)(p_2 \cdot p_3)$
$\nu_S \rightarrow \nu_\alpha + \nu_\alpha + \bar{\nu}_\alpha$	$1/2$	$64\,\vartheta_\alpha^2(p_1 \cdot p_4)(p_2 \cdot p_3)$
$\nu_S \rightarrow \nu_e + e^+ + e^-$	1	$128\,\vartheta_e^2[g_L^2(p_1 \cdot p_3)(p_2 \cdot p_4)+$ $g_R^2(p_1 \cdot p_4)(p_2 \cdot p_3) + g_L g_R m_e^2(p_1 \cdot p_2)]$
$\nu_S \rightarrow \nu_{\mu(\tau)} + e^+ + e^-$	1	$128\,\vartheta_{\mu(\tau)}^2[\tilde{g}_L^2(p_1 \cdot p_3)(p_2 \cdot p_4)+$ $g_R^2(p_1 \cdot p_4)(p_2 \cdot p_3) + \tilde{g}_L g_R m_e^2(p_1 \cdot p_2)]$

Table 4. Squared matrix elements for *decays* of sterile neutrinos ν_S. Here S is the symmetrization factor; $\alpha, \beta = e, \mu, \tau$; $\alpha \neq \beta$. ϑ_α is the mixing angle of sterile neutrino with ν_α. The results are both for Majorana and Dirac neutrinos, for details see text.

C Neutrino oscillations

The active neutrinos of different flavours ν_e, ν_μ, ν_τ are related to the mass eigen-state basis ν_1, ν_2, ν_3 via a non-diagonal Pontecorvo-Maki-Nakagava-Sakata (PMNS) matrix V $|\nu_\alpha\rangle = \sum V_{\alpha i} |\nu_i\rangle$ (see e.g. [58] for reviews):

$$V = \begin{pmatrix} 1 & 0 & 0 \\ 0 & c_{23} & s_{23} \\ 0 & -s_{23} & c_{23} \end{pmatrix} \begin{pmatrix} c_{13} & 0 & s_{13} \\ 0 & e^{i\phi} & 0 \\ -s_{13} & 0 & c_{13} \end{pmatrix} \begin{pmatrix} c_{12} & s_{12} & 0 \\ -s_{12} & c_{12} & 0 \\ 0 & 0 & 1 \end{pmatrix}.$$

here $c_{ij} = \cos\theta_{ij}$ and $s_{ij} = \sin\theta_{ij}$ are functions of the active-active neutrino mixing angles θ_{ij}.

Exact treatment of active neutrino oscillation in the early Universe is a difficult task (see e.g. [59–61]) Characteristic timescale of oscillation between i and j mass eigen-states for a neutrino with energy E is [58]

$$\tau_{ij} = \frac{4\pi E}{|m_i^2 - m_j^2|} \approx 8.3 \times 10^{-6} \text{s} \; \frac{E}{\text{MeV}} \frac{10^{-3} \text{ eV}^2}{|m_i^2 - m_j^2|} \tag{C.1}$$

Average energy of relativistic Fermi particles in equilibrium is $\langle E \rangle = 3.15 T$ [33]. Applying this relation to active neutrinos and using their measured mass differences [62] $m_2^2 - m_1^2 \approx 7.6 \times 10^{-5} \text{ eV}^2$, $|m_3^2 - m_1^2| \approx 2.5 \times 10^{-3} \text{ eV}^2$, we obtain

$$\tau_{12} \approx 1.0 \times 10^{-3} \sec \frac{T}{3 \text{ MeV}} \;, \;\; \tau_{13} \approx 3.1 \times 10^{-5} \sec \frac{T}{3 \text{ MeV}} \;, \tag{C.2}$$

provided that influence of the surrounding environment on neutrino propagation is neglected. One sees therefore that about the moment active neutrino decouples $T \simeq 3$ MeV typical oscillation timescales are much smaller than the Hubble expansion time given by eq. (2.2)

$$\tau_H = \sqrt{\frac{15}{4\pi^3 g_* G_N T^4}} \simeq 0.16 \sec \left(\frac{3 \text{ MeV}}{T}\right)^2 . \tag{C.3}$$

Here $g_* \approx 11$ (at $T \sim$ MeV) [33] is the so-called number of relativistic species that enters energy-temperature relation $\rho = \frac{\pi^2 g_* T^4}{30}$. Therefore, active neutrinos oscillate many times between the subsequent reactions involving them. In quantitative terms it means that probabilities $P_{\alpha\beta}$ to transform from flavour α to flavour β are oscillating functions of time. In realistic situation neutrinos do not have a definite momentum but are created in wave packets that are superpositions of states which have one. Since oscillation periods are momentum-dependent according to eq. (C.1), each state in the superposition will have his own period. Therefore after sufficiently many periods initial phases characterizing superposition will change, and there is no reason for the phase changes to be correlated with each other. So the decoherence of states is what happens. This phenomenon can be described effectively by averaging transition probabilities $P_{\alpha\beta}$ over time. Resulting expressions are [58]

$$P_{ee} = 1 - \frac{1}{2}(\sin^2 2\theta_{13} + \cos^4 \theta_{13} \sin^2 2\theta_{12}) \tag{C.4a}$$

$$P_{e\mu} = P_{\mu e} = \frac{1}{2} \cos^2 \theta_{13} \sin^2 2\theta_{12} \tag{C.4b}$$

$$P_{e\tau} = P_{\tau e} = \sin^2 \theta_{13} \cos^2 \theta_{13} \left(2 - \frac{1}{2} \sin^2 2\theta_{12} \right) \tag{C.4c}$$

$$P_{\mu\mu} = 1 - \frac{1}{2} \sin^2 2\theta_{12} \tag{C.4d}$$

$$P_{\mu\tau} = P_{\tau\mu} = \frac{1}{2} \sin^2 \theta_{13} \sin^2 2\theta_{12} \tag{C.4e}$$

$$P_{\tau\tau} = 1 - \sin^2 \theta_{13} \left(2 \cos^2 \theta_{13} + \frac{1}{2} \sin^2 \theta_{13} \sin^2 2\theta_{12} \right) \tag{C.4f}$$

To understand what happens with a neutrino, consider example of electron-neutrino created in electron-positron annihilation. At the production time this particle has probability 1 to oscillate into ν_e and zero for other final state. After long enough time for many oscillations to happen and before the time when a collision with other particle becomes quite probable, the decoherence comes into play. So now we may find the ν_e with probability P_{ee}, ν_μ with probability $P_{e\mu}$ and ν_τ with $P_{e\tau}$. The production rate of the initial specimen per unit time is proportional to collision integral I_e, according to the Boltzmann equation (2.7). But the actual number of produced electron neutrinos is actually reduced by factor P_{ee}. And even if (consider this hypothetical situation) muon neutrino does not interact with plasma, it will be anyway produced, at rate $P_{e\mu}I_e$. Generalization to other neutrino flavours leads us to conclusion that the modified Boltzmann equation

$$\frac{df_\alpha}{dt} = \sum P_{\alpha\beta} I_\beta \tag{C.5}$$

describes neutrino dynamics correctly (that is not the case for the initial equation (2.7)). For the actual computations we use the following experimental best-fit values: $\sin^2 \theta_{12} = 0.31$, $\sin^2 \theta_{23} = 0.52$ from [62], and $\sin^2 2\theta_{13} = 0.09$ from the Daya Bay [63]. The latter number is close to the result $\sin^2 2\theta_{13} = 0.11$ indicated by another recent experiment, RENO [64].

However, in dense medium oscillations proceed differently due to considerable effects of the plasma on properties of a single particle. Still, the phenomenon can be described by the formalism of the PMNS matrix. The difference is that mixing parameters together with masses now depend on properties of the environment. In case of plasma close to equilibrium with no non-trivial conserving charges present the parameter describing it is the temperature. So the parameters of the PMNS become *temperature-dependent*. In language of the effective Hamiltonian approach the system of three neutrinos is described by the addition of medium potential ΔH_M to the Hamiltonian H_V of the system in vacuum [65]

$$H_M = H_V + \Delta H_M, \quad H_V = \frac{1}{2E} V^* \text{diag}(m_1^2, m_2^2, m_3^2) V^\dagger , \tag{C.6}$$

where E is the neutrino energy. Diagonalization of the total propagation Hamiltonian H_M gives effective masses and mixings.

The medium potential comprises effects of neutrino interactions. Since neutrinos take part only in charged- and neutral-current interactions, matter potential has two terms ΔH_{CC}

and ΔH_{NC}, respectively. All neutrinos couple to neutral currents identically, so ΔH_{NC} is proportional to unit matrix. Therefore this term just renormalizes energy, and does not affect oscillations. In contrast, the charged-current term is non-diagonal and is present only for ν_e. The reason is that due to abundance of electrons in plasma, ν_e couples effectively to charged currents, while at temperatures below the muon's mass there is no significant contribution of muons and tau-leptons to realize coupling of other neutrinos to W boson.

Explicitly matter potential is [58]

$$\Delta H_{CC} = -\frac{14\sqrt{2}G_F}{45M_W^2} \ E \ T^4 \ \mathrm{diag}(1,0,0) \tag{C.7}$$

in the flavour neutrino basis $(\nu_e, \nu_\mu, \nu_\tau)$. M_W is the mass of the W-boson.

So far we have dropped sterile neutrinos from consideration. But their mixing properties are also altered in hot plasma. Using the approach of the effective Hamiltonian for them, one finds that their effective mixing angles in medium θ_M differ from that in vacuum θ_V as [65]

$$\frac{\theta_M - \theta_V}{\theta_V} \sim \frac{G_F T^5}{M_W^2 M_S^2} \sim 10^{-11} \times \left(\frac{T}{100\,\mathrm{MeV}}\right)^6 \ \left(\frac{10\,\mathrm{MeV}}{M_S}\right)^2 \tag{C.8}$$

for small mixing angles θ_V. Therefore the mixing angle is not altered significantly for sterile neutrinos and matter effects are negligible for their dynamics.

References

[1] Y. Izotov and T. Thuan, *The primordial abundance of 4He: evidence for non-standard big bang nucleosynthesis*, *Astrophys. J.* **710** (2010) L67 [arXiv:1001.4440] [INSPIRE].

[2] WMAP collaboration, E. Komatsu et al., *Seven-Year Wilkinson Microwave Anisotropy Probe (WMAP) Observations: Cosmological Interpretation*, *Astrophys. J. Suppl.* **192** (2011) 18 [arXiv:1001.4538] [INSPIRE].

[3] R. Alpher, H. Bethe and G. Gamow, *The origin of chemical elements*, *Phys. Rev.* **73** (1948) 803 [INSPIRE].

[4] F. Iocco, G. Mangano, G. Miele, O. Pisanti and P.D. Serpico, *Primordial Nucleosynthesis: from precision cosmology to fundamental physics*, *Phys. Rept.* **472** (2009) 1 [arXiv:0809.0631] [INSPIRE].

[5] G. Steigman, *Primordial Nucleosynthesis in the Precision Cosmology Era*, *Ann. Rev. Nucl. Part. Sci.* **57** (2007) 463 [arXiv:0712.1100] [INSPIRE].

[6] M. Pospelov and J. Pradler, *Big Bang Nucleosynthesis as a Probe of New Physics*, *Ann. Rev. Nucl. Part. Sci.* **60** (2010) 539 [arXiv:1011.1054] [INSPIRE].

[7] A. Boyarsky, O. Ruchayskiy and M. Shaposhnikov, *The role of sterile neutrinos in cosmology and astrophysics*, *Ann. Rev. Nucl. Part. Sci.* **59** (2009) 191 [arXiv:0901.0011] [INSPIRE].

[8] A. Kusenko, *Sterile neutrinos: the dark side of the light fermions*, *Phys. Rept.* **481** (2009) 1 [arXiv:0906.2968] [INSPIRE].

[9] E.K. Akhmedov, V. Rubakov and A.Y. Smirnov, *Baryogenesis via neutrino oscillations*, *Phys. Rev. Lett.* **81** (1998) 1359 [hep-ph/9803255] [INSPIRE].

[10] T. Asaka, S. Blanchet and M. Shaposhnikov, *The nuMSM, dark matter and neutrino masses*, *Phys. Lett.* **B 631** (2005) 151 [hep-ph/0503065] [INSPIRE].

[11] T. Asaka and M. Shaposhnikov, *The nuMSM, dark matter and baryon asymmetry of the universe*, *Phys. Lett.* **B 620** (2005) 17 [hep-ph/0505013] [INSPIRE].

[12] M. Shaposhnikov, *The nuMSM, leptonic asymmetries and properties of singlet fermions*, *JHEP* **08** (2008) 008 [arXiv:0804.4542] [inSPIRE].

[13] L. Canetti and M. Shaposhnikov, *Baryon asymmetry of the Universe in the NuMSM*, *JCAP* **09** (2010) 001 [arXiv:1006.0133] [inSPIRE].

[14] M. Laine and M. Shaposhnikov, *Sterile neutrino dark matter as a consequence of nuMSM-induced lepton asymmetry*, *JCAP* **06** (2008) 031 [arXiv:0804.4543] [inSPIRE].

[15] A. Dolgov, S. Hansen, G. Raffelt and D. Semikoz, *Cosmological and astrophysical bounds on a heavy sterile neutrino and the KARMEN anomaly*, *Nucl. Phys.* **B 580** (2000) 331 [hep-ph/0002223] [inSPIRE].

[16] A. Dolgov, S. Hansen, G. Raffelt and D. Semikoz, *Heavy sterile neutrinos: Bounds from big bang nucleosynthesis and SN1987A*, *Nucl. Phys.* **B 590** (2000) 562 [hep-ph/0008138] [inSPIRE].

[17] C.J. Smith, G.M. Fuller and M.S. Smith, *Big Bang Nucleosynthesis with Independent Neutrino Distribution Functions*, *Phys. Rev.* **D 79** (2009) 105001 [arXiv:0812.1253] [inSPIRE].

[18] G.M. Fuller, C.T. Kishimoto and A. Kusenko, *Heavy sterile neutrinos, entropy and relativistic energy production and the relic neutrino background*, arXiv:1110.6479 [inSPIRE].

[19] A. Dolgov, S. Hansen and D. Semikoz, *Impact of massive tau neutrinos on primordial nucleosynthesis. Exact calculations*, *Nucl. Phys.* **B 524** (1998) 621 [hep-ph/9712284] [inSPIRE].

[20] A. Dolgov and D. Kirilova, *Nonequilibrium decays of light particles and the primordial nucleosynthesis*, *Int. J. Mod. Phys.* **A 3** (1988) 267 [inSPIRE].

[21] M. Kawasaki et al., *Big bang nucleosynthesis constraints on the tau-neutrino mass*, *Nucl. Phys.* **B 419** (1994) 105 [inSPIRE].

[22] M. Kawasaki, K. Kohri and N. Sugiyama, *MeV scale reheating temperature and thermalization of neutrino background*, *Phys. Rev.* **D 62** (2000) 023506 [astro-ph/0002127] [inSPIRE].

[23] S. Hannestad, *What is the lowest possible reheating temperature?*, *Phys. Rev.* **D 70** (2004) 043506 [astro-ph/0403291] [inSPIRE].

[24] A. Dolgov, S. Hansen and D. Semikoz, *Nonequilibrium corrections to the spectra of massless neutrinos in the early universe: Addendum*, *Nucl. Phys.* **B 543** (1999) 269 [hep-ph/9805467] [inSPIRE].

[25] A. Dolgov, S. Hansen and D. Semikoz, *Nonequilibrium corrections to the spectra of massless neutrinos in the early universe*, *Nucl. Phys.* **B 503** (1997) 426 [hep-ph/9703315] [inSPIRE].

[26] D. Gorbunov and M. Shaposhnikov, *How to find neutral leptons of the nuMSM?*, *JHEP* **10** (2007) 015 [arXiv:0705.1729] [inSPIRE].

[27] Particle Data Group collaboration, K. Nakamura et al., *Review of particle physics*, *J. Phys.* **G 37** (2010) 075021 [inSPIRE].

[28] A. Serebrov and A. Fomin, *Neutron lifetime from a new evaluation of ultracold neutron storage experiments*, *Phys. Rev.* **C 82** (2010) 035501 [arXiv:1005.4312] [inSPIRE].

[29] J. Lesgourgues and S. Pastor, *Cosmological implications of a relic neutrino asymmetry*, *Phys. Rev.* **D 60** (1999) 103521 [hep-ph/9904411] [inSPIRE].

[30] P.D. Serpico and G.G. Raffelt, *Lepton asymmetry and primordial nucleosynthesis in the era of precision cosmology*, *Phys. Rev.* **D 71** (2005) 127301 [astro-ph/0506162] [inSPIRE].

[31] C.J. Smith, G.M. Fuller, C.T. Kishimoto and K.N. Abazajian, *Light Element Signatures of Sterile Neutrinos and Cosmological Lepton Numbers*, *Phys. Rev.* **D 74** (2006) 085008 [astro-ph/0608377] [inSPIRE].

[32] G. Mangano, G. Miele, S. Pastor, O. Pisanti and S. Sarikas, *Constraining the cosmic radiation density due to lepton number with Big Bang Nucleosynthesis*, *JCAP* **03** (2011) 035 [arXiv:1011.0916] [INSPIRE].

[33] E. Kolb and M. Turner, *The Early Universe*, Addison-Wesley, Reading U.S.A. (1990).

[34] F. Bezrukov, D. Gorbunov and M. Shaposhnikov, *On initial conditions for the Hot Big Bang*, *JCAP* **06** (2009) 029 [arXiv:0812.3622] [INSPIRE].

[35] L. Kawano, *Let's Go: Early Universe. Guide to Primordial Nucleosynthesis Programming*, FERMILAB-PUB-88-034-A (1988).

[36] L. Kawano, *Let's go: Early universe. 2. Primordial nucleosynthesis: the computer way*, FERMILAB-PUB-92/04-A (1992), http://ntrs.nasa.gov/search.jsp?R=19920015920.

[37] P.J. Kernan and L.M. Krauss, *Refined big bang nucleosynthesis constraints on Omega (baryon) and N (neutrino)*, *Phys. Rev. Lett.* **72** (1994) 3309 [astro-ph/9402010] [INSPIRE].

[38] R.N. Boyd, C.R. Brune, G.M. Fuller and C.J. Smith, *New Nuclear Physics for Big Bang Nucleosynthesis*, *Phys. Rev.* **D 82** (2010) 105005 [arXiv:1008.0848] [INSPIRE].

[39] G.M. Fuller and C.J. Smith, *Nuclear weak interaction rates in primordial nucleosynthesis*, *Phys. Rev.* **D 82** (2010) 125017 [arXiv:1009.0277] [INSPIRE].

[40] A. Coc, S. Goriely, Y. Xu, M. Saimpert and E. Vangioni, *Standard Big-Bang Nucleosynthesis up to CNO with an improved extended nuclear network*, *Astrophys. J.* **744** (2012) 158 [arXiv:1107.1117] [INSPIRE].

[41] S. Sarkar, *Big bang nucleosynthesis and physics beyond the standard model*, *Rept. Prog. Phys.* **59** (1996) 1493 [hep-ph/9602260] [INSPIRE].

[42] O. Pisanti et al., *PArthENoPE: Public Algorithm Evaluating the Nucleosynthesis of Primordial Elements*, *Comput. Phys. Commun.* **178** (2008) 956 [arXiv:0705.0290] [INSPIRE].

[43] E. Aver, K.A. Olive and E.D. Skillman, *An MCMC determination of the primordial helium abundance*, *JCAP* **04** (2012) 004 [arXiv:1112.3713] [INSPIRE].

[44] G. Mangano and P.D. Serpico, *A robust upper limit on N_{eff} from BBN, circa 2011*, *Phys. Lett.* **B 701** (2011) 296 [arXiv:1103.1261] [INSPIRE].

[45] M. Peimbert, V. Luridiana and A. Peimbert, *Revised Primordial Helium Abundance Based on New Atomic Data*, *Astrophys. J.* **666** (2007) 636 [astro-ph/0701580] [INSPIRE].

[46] J. Dunkley et al., *The Atacama Cosmology Telescope: Cosmological Parameters from the 2008 Power Spectra*, *Astrophys. J.* **739** (2011) 52 [arXiv:1009.0866] [INSPIRE].

[47] R. Keisler et al., *A Measurement of the Damping Tail of the Cosmic Microwave Background Power Spectrum with the South Pole Telescope*, *Astrophys. J.* **743** (2011) 28 [arXiv:1105.3182] [INSPIRE].

[48] G. Gelmini, S. Palomares-Ruiz and S. Pascoli, *Low reheating temperature and the visible sterile neutrino*, *Phys. Rev. Lett.* **93** (2004) 081302 [astro-ph/0403323] [INSPIRE].

[49] G.B. Gelmini, E. Osoba and S. Palomares-Ruiz, *Inert-Sterile Neutrino: Cold or Warm Dark Matter Candidate*, *Phys. Rev.* **D 81** (2010) 063529 [arXiv:0912.2478] [INSPIRE].

[50] G.M. Fuller, A. Kusenko and K. Petraki, *Heavy sterile neutrinos and supernova explosions*, *Phys. Lett.* **B 670** (2009) 281 [arXiv:0806.4273] [INSPIRE].

[51] B. Benson et al., *Cosmological Constraints from Sunyaev-Zel'dovich-Selected Clusters with X-ray Observations in the First 178 Square Degrees of the South Pole Telescope Survey*, arXiv:1112.5435 [INSPIRE].

[52] M. Moresco, L. Verde, L. Pozzetti, R. Jimenez and A. Cimatti, *New constraints on cosmological parameters and neutrino properties using the expansion rate of the Universe to z ∼ 1.75*, *JCAP* **07** (2012) 053 [`arXiv:1201.6658`] [ɪɴSPIRE].

[53] T. Asaka, M. Shaposhnikov and A. Kusenko, *Opening a new window for warm dark matter*, *Phys. Lett.* **B 638** (2006) 401 [`hep-ph/0602150`] [ɪɴSPIRE].

[54] T. Asaka, S. Eijima and H. Ishida, *Mixing of Active and Sterile Neutrinos*, *JHEP* **04** (2011) 011 [`arXiv:1101.1382`] [ɪɴSPIRE].

[55] O. Ruchayskiy and A. Ivashko, *Experimental bounds on sterile neutrino mixing angles*, *JHEP* **06** (2012) 100 [`arXiv:1112.3319`] [ɪɴSPIRE].

[56] J. Racle, *Deriving bounds on interactions of numsm sterile neutrinos using primordial nucleosynthesis*, MSc Thesis, École Polytechnique Fédérale de Lausanne (EPFL), Lausanne Switzerland (2008).

[57] G. Mangano et al., *Relic neutrino decoupling including flavor oscillations*, *Nucl. Phys.* **B 729** (2005) 221 [`hep-ph/0506164`] [ɪɴSPIRE].

[58] A. Strumia and F. Vissani, *Neutrino masses and mixings and...*, `hep-ph/0606054` [ɪɴSPIRE].

[59] A. Dolgov et al., *Cosmological bounds on neutrino degeneracy improved by flavor oscillations*, *Nucl. Phys.* **B 632** (2002) 363 [`hep-ph/0201287`] [ɪɴSPIRE].

[60] A. Dolgov and F. Villante, *BBN bounds on active sterile neutrino mixing*, *Nucl. Phys.* **B 679** (2004) 261 [`hep-ph/0308083`] [ɪɴSPIRE].

[61] D. Kirilova, *Non-equilibrium neutrino in the early universe plasma*, *AIP Conf. Proc.* **1121** (2009) 83 [ɪɴSPIRE].

[62] T. Schwetz, M. Tortola and J. Valle, *Where we are on θ_{13}: addendum to 'Global neutrino data and recent reactor fluxes: status of three-flavour oscillation parameters'*, *New J. Phys.* **13** (2011) 109401 [`arXiv:1108.1376`] [ɪɴSPIRE].

[63] DAYA-BAY collaboration, F. An et al., *Observation of electron-antineutrino disappearance at Daya Bay*, *Phys. Rev. Lett.* **108** (2012) 171803 [`arXiv:1203.1669`] [ɪɴSPIRE].

[64] RENO collaboration, J. Ahn et al., *Observation of Reactor Electron Antineutrino Disappearance in the RENO Experiment*, *Phys. Rev. Lett.* **108** (2012) 191802 [`arXiv:1204.0626`] [ɪɴSPIRE].

[65] D. Notzold and G. Raffelt, *Neutrino Dispersion at Finite Temperature and Density*, *Nucl. Phys.* **B 307** (1988) 924 [ɪɴSPIRE].